A three-dimensional model of an air bubble curtain in offshore pile driving

Peng, Yaxi; Tsouvalas, Apostolos

DOI
10.1088/1742-6596/2647/23/232006

Publication date
2024

Document Version
Final published version

Published in
Journal of Physics: Conference Series

Journal of Physics: Conference Series

PAPER • **OPEN ACCESS**

A three-dimensional model of an air bubble curtain in offshore pile driving

To cite this article: Yaxi Peng and Apostolos Tsouvalas 2024 *J. Phys.: Conf. Ser.* **2647** 232006

Journal of Physics: Conference Series **2647** (2024) 232006 doi:10.1088/1742-6596/2647/23/232006

A three-dimensional model of an air bubble curtain in offshore pile driving

Yaxi Peng, Apostolos Tsouvalas

Department of Structural Engineering, Delft University of Technology, Stevinweg 1, 2628 CN, Delft, Netherlands

E-mail: y.peng@tudelft.nl

Abstract. With the growing demand for renewable energy, an increased number of offshore wind farms are planned to be constructed in the coming decades. The monopile is the main foundation of offshore wind turbines in shallow waters while the installation process itself takes place with large hydraulic impact hammers. This process is accompanied by significant underwater noise pollution which can hinder the life of mammals and fish. To protect the marine ecosystem, strict sound thresholds are imposed by regulators in many countries. Among the various noise mitigation systems available, the air-bubble curtain is the most widely applied one. While several models exist which aim to describe the mitigation performance of air-bubble curtains, they all assume a cylindrically symmetric wave field. However, it is well known that the performance of the air-bubble curtains can vary significantly in azimuth due to the inherent variations in the airflow circulation through the perforated pipes positioned on the seabed surface. This paper presents a new model which is based on a multi-physics approach and considers the three-dimensional behavior of the air-bubble curtain system. The complete model consists of three modules: (i) a hydrodynamic model for capturing the characteristics of bubble clouds in varying development phases through depth; (ii) an acoustic model for predicting the sound insertion loss of the air-bubble curtain; and (iii) a vibroacoustic model for the prediction of underwater noise from pile driving which is coupled to the acoustic model in (iii) through a three-dimensional boundary integral formulation. The boundary integral model is validated against a finite element model. The model allows for a comparison of various mitigation scenarios including the perfectly deployed air bubble curtain system, i.e.no azimuth-dependent field, and an imperfect system due to possible leakage in the bubbly sound barrier along the circumference of the hose.

1. Introduction

Offshore wind farms supply an increasingly significant amount of renewable energy around the world. The main foundations of the offshore wind turbines are monopiles. The installation of the foundations requires hydraulic impact hammering to drive the pile into the seabed, which produces high-level of noise underwater [1]. The noise pollution due to the impact piling has raised critical environmental concern for endangering the life of marine mammals [2, 3]. Underwater noise has been realized as a sound pollution causing migrating, foraging and other behavioral changes in marine mammals and fishes [2]. Noise mitigation systems are usually used to keep the noise levels to acceptable thresholds, among which the air bubble curtains are mostly widely adopted system in offshore installation projects [5, 6]. The bubble curtain systems are also commonly used for the prevention of the spreading of particles and other contaminants, such as oil and salinity. An

environmental assessment of the impact of the noise is often required before the installation and the noise levels are monitored during the construction activities. The prediction of the noise levels is critical in the assessment process so as to provide the expected sound levels and to examine the environmental risk to comply with the regulations. The quantitive assessment of the noise requires analysis of the marine environmental conditions, the noise generation and propagation from impact pile driving, the noise reduction performance of the air bubble curtains and other noise mitigation systems. There is a critical need for an assessment tool that is able to capturing all these aspects.

Many studies have been performed on modeling the generation and propagation of impact piling noise [7, 8, 9, 10, 11, 12]. In addition, there is an increasing interest in investigating the main mechanism of the bubble curtains and predicting the acoustic performance of the system when applied to offshore pile driving [6, 14, 15]. The DBBC system is usually modeled as a non-reflecting impedance boundary condition around the pile in the finite element models [16]. In the semi-analytical model by Tsouvalas and Metrikine [6], the air-bubble curtain is considered as a more realistic homogeneous medium with a constant thickness over the entire water depth. Based on the dynamic sub-structuring approach, the modeling domain is divided into the pile, water, soil and bubbly mixture sub-domains [6]. The technique allows the coupling of the complete system through the interface between the structure, surrounding medium and the bubble curtains. Sertlek and Tsouvalas developed a coupled mode theory based solution to model the wave propagation through an air bubble curtain, which is based on the orthogonality of the acousto-elastic modes [17]. To understand the bubble dynamics within the bubble curtains, a Computational Fluid Dynamic (CFD) model was proposed by Gottsche [18]. The bubble distribution and gas volume fraction are determined with a CFD model. The noise radiation during pile driving is simulated by Finite Element Analysis and an Effective Medium Approach in the near field, while a Parabolic Equation model is employed in the far field. However, the bubble distribution is assumed constant over the entire domain, which is not valid for accurate predictions. An integral approach for deriving the local distribution of the air fraction was developed by Bohne in 2019 [13]. The model presents a local distribution of the effective wavenumber, which can be used in the acoustic model for determining the transmission characteristic of the bubble curtain. The bubble formation process directly at the nozzle is later incorporated into the model in [14], which is coupled to the fluid mechanism and allows the bubble generation to a greater distance from the nozzle. Measurement has been conducted to examine the hydraulic properties of the bubble curtain including the local void fractions and bubble size distributions [19].

In this paper, the proposed method provides a foundation for evaluating the three-dimensional behaviour of the air bubble curtain system. This work is structured as follows, the formulation of the problem for incorporating the azimuthal dependent behaviour of the air-bubble curtain is presented. Then, the validation study for a theoretical case is performed with the comparison to the numerical results from finite-element model. Underwater noise prognosis is performed using realistic data from an offshore installation campaign in 2018, a non-fully blocked waterborne path with gaps in pre-defined angles is examined as a sample problem. The prediction results are compared to the free-field noise prediction and the scenario with full-blocked water borne path at the position of the air bubble curtain. The proposed modeling approach can be easily extended by incorporating a realistic transmission coefficient of the bubbly layer through the azimuthal coordinate.

2. Methodology

A numerical approach is proposed for evaluating the noise emission from the impact pile driving with the use of the air-bubble curtain system. The complete modeling chain consists of the following modules: (i) a hydrodynamic model for capturing the

characteristics of bubble clouds in varying development phases through the water depth; (ii) an acoustic model for predicting the sound insertion loss of the air-bubble curtain; and (iii) a vibro-acoustic model for the prediction of underwater noise from pile driving which is coupled to the acoustic model in (iii) through a three-dimensional boundary integral formulation. The hydrodynamic and the acoustic models have been described into great details in [14, 15]. In this section, we focus on the coupled dynamic problem in an axisymmetric acousto-elastic medium with non-axiymmetric boundary conditions at the position of the bubble curtain.

2.1. Three dimensional Green's Function

A symmetric cylindrical coordinate system $\boldsymbol{r} = (r, \theta, z)$ is introduced and $\boldsymbol{r_s} = (r_s, \theta_s, z_s)$ indicates the location of the source at the position of the bubble curtain. The displacement field is describe by $\boldsymbol{u} = [u, v, w]$ and p_f denotes the pressure in the fluid. The equation of motion for the acousto-elastic medium is given as[12]:

$$(\lambda + 2\mu)\nabla(\nabla \cdot \boldsymbol{u}) - \mu\nabla \times (\nabla \times \boldsymbol{u}) = \rho\ddot{\boldsymbol{u}} \tag{1}$$

$$\nabla^2 p_f - \frac{1}{c_f^2}\ddot{p_f} = 0 \tag{2}$$

A regular decomposition is applied to the displacement field as [20],

$$\boldsymbol{u} = \nabla\phi + \nabla \times [\chi \boldsymbol{e}_z + \nabla \times [\eta \boldsymbol{e}_z]] \tag{3}$$

Now, the acousto-elastic wave equations can be solved by finding the solutions to a set of scalar potential wave equations [20],

$$[\nabla^2 + k_f^2(z)]\tilde{\phi}_f(r, \theta, z) = 0 \tag{4}$$

$$[\nabla^2 + k_p^2(z)]\tilde{\phi}(r, \theta, z) = 0 \tag{5}$$

$$[\nabla^2 + k_s^2(z)]\tilde{\chi}(r, \theta, z) = 0 \tag{6}$$

$$[\nabla^2 + k_s^2(z)]\tilde{\eta}(r, \theta, z) = 0 \tag{7}$$

For the solutions of Eq.(4-7), it is convenient to employ an angular Fourier decomposition

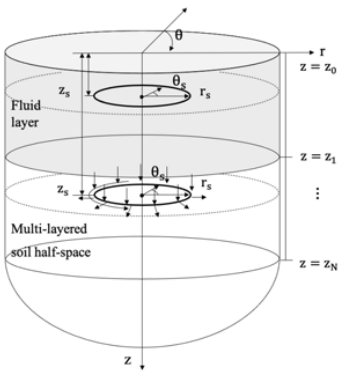

Figure 1. Geometry of the model for ring load for the three dimensional Green's function.

in the form of

$$\tilde{\phi}_f(r,\theta,z) = \sum_{m=-\infty}^{\infty} \phi_{fm}(r,z)e^{im\theta}, \quad \tilde{\phi}(r,\theta,z) = \sum_{m=-\infty}^{\infty} \phi_m(r,z)e^{im\theta} \tag{8}$$

$$\tilde{\chi}(r,\theta,z) = \sum_{m=-\infty}^{\infty} \chi_m(r,z)e^{im\theta}, \quad \tilde{\eta}(r,\theta,z) = \sum_{m=-\infty}^{\infty} \eta_m(r,z)e^{im\theta} \tag{9}$$

in which the m-th series coefficients $\Phi_m = [\phi_{fm},\, \phi_m,\, \chi_m,\, \eta_m]$ is given by:

$$\Phi_m(r,z) = \frac{1}{2\pi}\int_0^{2\pi} \tilde{\Phi}(r,\theta,z)e^{-im\theta}d\theta \tag{10}$$

with $\theta = [0, 2\pi]$. Applying the Hankel transform pairs to the m-th order potential coefficients $\hat{\Phi}_m(r,z)$,

$$\Phi_m(r,z) = \int_0^{\infty} \hat{\Phi}_m(k_r,z)k_r J_m(k_r r)dk_r \tag{11}$$

$$\hat{\Phi}_m(k_r,z) = \int_0^{\infty} \Phi_m(r,z)(k_r,z)r J_m(k_r r)dr \tag{12}$$

in which a "hat" denotes a physical quantity in the wavenumber domain. The governing equations are reduced to the depth-dependent wave equations as:

$$\frac{d^2}{dz^2}\hat{\phi}_{fm}(k_r,z) + (k_f^2 - k_r^2)\hat{\phi}_{fm}(k_r,z) = 0 \tag{13}$$

$$\frac{d^2}{dz^2}\hat{\phi}_m(k_r,z) + (k_p^2 - k_r^2)\hat{\phi}_m(k_r,z) = 0 \tag{14}$$

$$\frac{d^2}{dz^2}\hat{\chi}_m(k_r,z) + (k_s^2 - k_r^2)\hat{\chi}_m(k_r,z) = 0 \tag{15}$$

$$\frac{d^2}{dz^2}\hat{\eta}_m(k_r,z) + (k_s^2 - k_r^2)\hat{\eta}_m(k_r,z) = 0 \tag{16}$$

The general solutions for the above potential functions can be written as

$$\hat{\Phi}_m(k_r,z) = A_{\xi 1}(k_r)e^{ik_{z\xi}z} + A_{\xi 2}(k_r)e^{-ik_{z\xi}z} \tag{17}$$

For different type of transfer functions and various number of circumferential order, a proper definition of angular Fourier transform is required to achieve good estimation in the solution in the m-th order. The transformed displacements $[\hat{u}_{r_m},\, \hat{u}_{\theta_m},\, \hat{u}_{r_m}]$ and stress-fields $[\hat{\tau}_{zz_m},\, \hat{\tau}_{zr_m},\, \hat{\tau}_{z\theta_m},\, \hat{\tau}_{rr_m},\, \hat{\tau}_{\theta\theta_m},\, \hat{\tau}_{r\theta_m},\,]$ can be obtained from the potential functions.

2.2. Transformed loading conditions

An arbitrarily distributed ring load in the fluid at a certain depth z_s can be expressed by adding the source term directly in the governing Eq. 13, i.e.:

$$\frac{d^2}{dz^2}\hat{\phi}_{fm}(k_r,z) + (k_f^2 - k_r^2)\hat{\phi}_{fm}(k_r,z) = \frac{1}{-\rho\omega^2}\delta(z - z_s)\frac{J_m(k_r r_s)}{2\pi}\hat{P}_m \tag{18}$$

with the pressure source F_f in the fluid defined as:

$$F_f(r_s,\theta_s,z_s) = \sum_{m=-\infty}^{\infty} \hat{P}_m e^{im\theta_s}\frac{J_m(k_r r_s)}{2\pi} \tag{19}$$

For the soil, the arbitrarily distributed ring load on the plane z_s can be represented as a set of jump conditions across the interface. In the wavenumber domain, the transformed loading conditions are applied as follows:

$$\hat{\tau}_{22_m}(k_r, z_s+) - \hat{\tau}_{22_m}(k_r, z_s-) = \hat{Z}_m \frac{J_m(k_r r_s)}{2\pi} \tag{20}$$

$$\hat{\tau}_{21_m}(k_r, z_s+) - \hat{\tau}_{21_m}(k_r, z_s-) = \frac{\hat{Y}_m - \hat{X}_m}{2} \frac{J_m(k_r r_s)}{2\pi} \tag{21}$$

$$\hat{\tau}_{23_m}(k_r, z_s+) - \hat{\tau}_{23_m}(k_r, z_s-) = \frac{\hat{Y}_m + \hat{X}_m}{2} \frac{J_m(k_r r_s)}{2\pi} \tag{22}$$

with X_m and Y_m defined as:

$$\hat{X}_m = \hat{R}_m - i\hat{T}_m \tag{23}$$

$$\hat{Y}_m = \hat{R}_m + i\hat{T}_m \tag{24}$$

in which $\hat{R}_m$, $\hat{T}_m$ and $\hat{Z}_m$ are the source term based on the ring load in R, θ and Z directions and are defined in similar form as shown in Eq. 19. Now, the foregoing equations become decoupled into two sets of algebraic equations, one is related to the coupled P-SV wave propagation:

$$\hat{u}_{1_m}(k_r, z) = 2k_r(\hat{\phi}_m(z) + \hat{\eta}'_m(z)) \tag{25}$$

$$\hat{u}_{2_m}(k_r, z) = (\hat{\phi}'_m(z) + k_r^2 \hat{\eta}_m(z) \tag{26}$$

$$\hat{\tau}_{21_m}(k_r, z) = -2\mu k_r(2\hat{\phi}'_m(z) + 2\hat{\eta}''_m(z) + k_s^2 \hat{\eta}_m(z) + \hat{\eta}'_m(z)) \tag{27}$$

$$\hat{\tau}_{22_m}(k_r, z) = -\lambda k_p^2 \hat{\phi}_m(z) + 2\mu(k_s^2 \hat{\eta}'_m(z) + \hat{\phi}''_m(z) + \hat{\eta}''_m(z)) \tag{28}$$

$$\hat{\tau}_{33_m}(k_r, z) = -\lambda k_p^2 \hat{\phi}_m(z) \tag{29}$$

$$\hat{\tau}_{11_m}(k_r, z) = -\lambda k_p^2 \hat{\phi}_m(z) - 2\mu k_r^2(\hat{\eta}'_m(z) + \hat{\phi}_m(z)) \tag{30}$$

in which solely the potential functions $\hat{\phi}_m(z)$ and $\hat{\eta}_m(z)$ are involved. Another set of equations is obtained for the uncoupled SH wave propagation:

$$\hat{u}_{3_m}(k_r, z) = 2ik_r \hat{\chi}_m(z) \tag{31}$$

$$\hat{\tau}_{23_m}(k_r, z) = 2ik_r \mu \hat{\chi}'_m(z) \tag{32}$$

$$\hat{\tau}_{13_m}(k_r, z) = \mu k_r^2 \hat{\chi}_m(z) \tag{33}$$

in which the potential functions $\hat{\chi}_m(z)$ are to be determined. By applying the loading, boundary and interface conditions into both subsystems by assuming the following coefficients:

$$\hat{\phi}_{fm}(z) = A_{m,1} e^{ik_{zf}(z-D_1)} + A_{m,2} e^{-ik_{zf}z} \tag{34}$$

$$\hat{\phi}_m(z) = A_{m,4j-1} e^{ik_{zp}(z-D_{j+1})} + A_{m,4j} e^{-ik_{zp}(z-D_j)} \tag{35}$$

$$\hat{\chi}_m(z) = B_{m,2j-1} e^{ik_{zs}(z-D_{j+1})} + B_{m,2j} e^{-ik_{zs}(z-D_j)} \tag{36}$$

$$\hat{\eta}_m(z) = A_{m,4j+1} e^{ik_{zs}(z-D_{j+1})} + A_{m,4j+2} e^{-ik_{zs}(z-D_j)} \tag{37}$$

in which j indicates the index of soil layer and D_j and D_{j+1} indicate the depth of the upper and lower boundary of the soil layer j. When $j = N$, the multiplier of the exponents in the first term in Eqs. (35 - 37) vanish to ensure the radiation condition at $z \to \infty$.

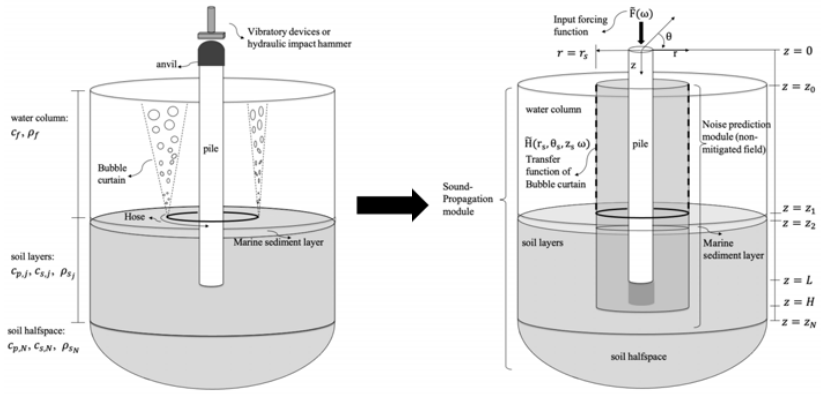

Figure 2. Schematic of the complete system (left) and the coupled model (right).

2.3. Boundary Intergal Equation method in three-dimensional field

The reduced boundary integral equation (BIE) for the three-dimensional boundary conditions is obtained as [21, 22]:

$$\begin{aligned}
&\hat{\boldsymbol{u}}^{\Xi}_{\alpha m}(r,z) = \\
&\int_{L^f} R_{bc}\left(\bar{U}^{\Xi f}_{\alpha r,m}(\boldsymbol{r},\boldsymbol{r}'_s)\cdot\hat{p}^{*}_{m}(z_s) - \bar{T}^{,\Xi f}_{\alpha r,m}(\boldsymbol{r},\boldsymbol{r}'_s)\cdot\hat{u}^{f*}_{rm}(z_s)\right)dL^f(r_s,z_s) \\
&+\sum_{\beta=r,\theta,z}\int_{L^s} R_{bc}\left(\bar{U}^{\Xi s}_{\alpha\beta,m}(\boldsymbol{r},\boldsymbol{r}'_s,\omega)\cdot\hat{t}^{\boldsymbol{n}}_{\beta}(z_s) - \bar{T}^{\boldsymbol{n},\Xi s}_{\alpha\beta,m}(\boldsymbol{r},\boldsymbol{r}'_s,\omega)\cdot\hat{u}_{\beta m}(z_s)\right)dL^s_s(r_s,z_s)
\end{aligned} \tag{38}$$

in which the Green's tensor $\bar{U}^{\Xi\Phi}_{\alpha\beta,m}$ and $\bar{T}^{,\Xi\Phi}_{\alpha\beta,m}$ are obtained from the potential functions based on the source location in either fluid or soil as given in Eq.34 - 37. The angular Fourier decomposition are employed in the boundary integral equation formulation, which enable the acceleration of computation. The source terms are obtained by solving the vibro-acoustic model for the prediction of underwater noise from pile driving [12].

3. Numerical Implementation

In this section, two numerical examples are examined in order to demonstrate the accuracy of the propose three-dimensional acousto-elastic boundary integral formulation. The first one is a theoretical benchmark problem, which is dealt with the radiation from a cylindrical surface in the fluid domain. The problem is solved by using the boundary integral approach with a pre-defined pressure and velocity distribution on the boundary. The second problem is based on an offshore wind farm in German North Sea with the use of double bubble curtain system.

3.1. Theoretical benchmark case

A fluid layer overlying an elastic half-space is modeled in COMSOL Multiphysics with a surface load indicating the non-symmetric loading condition. As the three-dimensional case in COMSOL require more computational effort due to the increased number of meshes, elements, the number of degree of freedoms and resulted modeling interaction in the MUMP solver, the size of the model is reduced compared to the previous case by decreasing the water depth and soil depth examined.

The θ dependent transfer function is defined in figure 4, which can be transformed into the complex Fourier domain as $\widehat{H}_m(r,z)$. The input parameters including the geometry

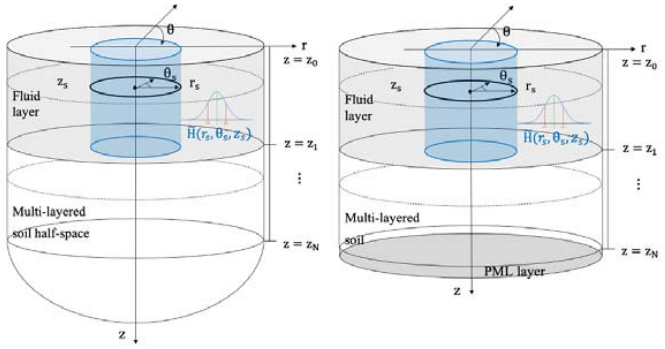

Figure 3. Geometry of the model for the validation of the boundary integrals formulations for a surface load positioned in the fluid domain as a pressure and velocity combined source.

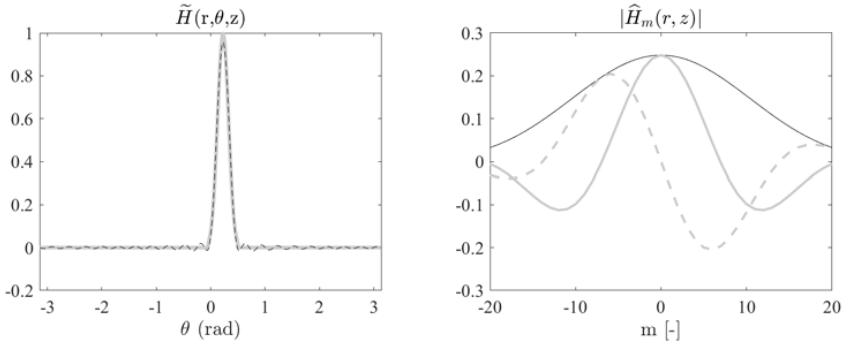

Figure 4. Non-fully blocked idealized noise cancelling screen: $\widetilde{H}(r,\theta,z)$ is the transmission coefficient and $\widehat{H}_m(r,z)$ is transformed complex Fourier coefficient with m-th order.

Table 1. Basic input parameters for the validation study.

Parameter	Depth	ρ	c_L	c_T	α_p	α_s
-	[m]	[kg/m^3]	[m/s]	[m/s]	$[dB/\lambda]$	$[dB/\lambda]$
Fluid	40	1000	1500	-	-	-
Bottom soil	∞	1888	1775	198	0.2	0.8

of the domain and the material properties are given. In the FE model, the soil half-space is substituted by a perfectly-matched layer to account for the radiation condition at $z \to \infty$. The comparison between the FEM model and semi-analytical model based on the boundary integral equation formulation are shown in figures 5 and 6. The Green's tensors are shown in figure 5, which are compared to the numerical results from FEM. It can be seen that the semi-analytical approach provide results in excellent agreement with the numerical solution.

3.2. Offshore wind farm in German North Sea

In this section, the case examined is based on an offshore wind farm foundation installation campaign in 2018 [12, 15]. The material properties, the geometry and the forcing function of the model are summarised in [15]. The forcing function is defined as the smoothed

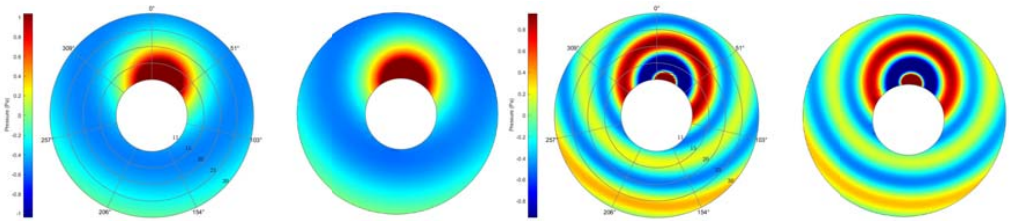

Figure 5. Comparison of Green's tensors from the proposed model (left) and FEM (right) at excitation frequencies 30 Hz (top) and 125 Hz (bottom) as indicated in Fig. 3for the mid of the water depth.

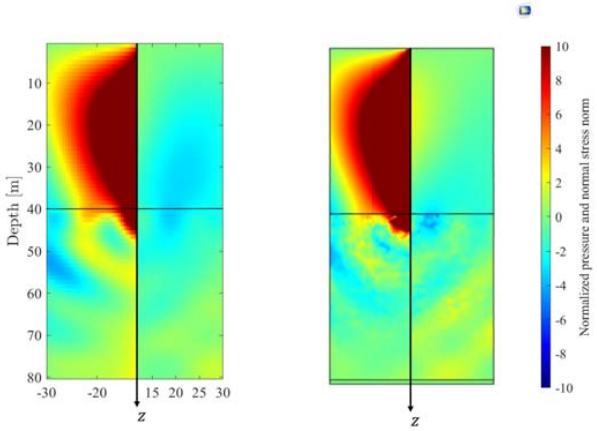

Figure 6. Comparison of Boundary Integral Formulation from the proposed model (left) and FEM (right) at excitation frequencies 30 Hz (top) as indicated in Fig. 3. The pressure field in the fluid and the normal stress of the soil σ_{zz} for $\theta = 15°$ (on the negative r axis) and 195° (on the positive r axis) are shown.

exponential impulse, which results in approximately 2000 kJ input energy into the pile. The seabed at this foundation consists of a thin marine sediment layer overlaying a stiff bottom soil half-space.

At this foundation, the DBBC system was deployed. The inner bubble curtain is positioned at 105m from the pile and the outer bubble curtain is positioned at 145m from the pile. In this analysis, the DBBC system will not be modeled explicitly but substituted by an ideal noise absorption function. A non-fully blockage of the water-borne path is examined with a gap as defined in figure 4.

The overall SEL and $L_{p,pk}$ for both unmitigated and mitigated fields are summarised in Table 2. The measured sound levels indicate a range of 14 to 17 dB noise reduction achieved by the DBBC system for both SEL and $L_{p,pk}$. The variation in the measurement indicate the 3 dB differences in both SEL and $L_{p,pk}$ at different azimuthal directions.

With the modeling of the perfect noise mitigation at the position of the outer bubble curtain, the maximum noise reduction levels are 30dB for both SEL and 34dB for $L_{p,pk}$. When a sound gap exists, the SEL deviates up to 1 dB from the receiver at $\theta = 0°$ of the field and up to 6 dB for the $L_{p,pk}$. The variation of the $L_{p,pk}$ in azimuth is much larger, while for SEL is less significant. As most of the energy is channeled through the seabed, the influence of the small gap over the water depth is less critical as it leads to an increase of 2 to 3 dB in the SEL. In order to examine the sensitivity of the DBBC system along the

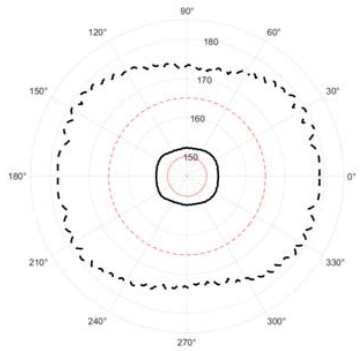

Figure 7. Azimuthal dependent SEL and $L_{p,pk}$ for partially blockage of the water borne path with a thin gap over the entire water depth: the red solid line indicates the SEL and the red dashed line reads the $L_{p,pk}$ for the fully blockage of the water borne transmission path; the black solid and dashed lines are SEL and $L_{p,pk}$ for partially blockage case.

Table 2. Noise mitigation assessment at the foundation. All values are given at a distance of 750m from the pile. SEL are given in the unit of dB re $1\mu\ Pa^2s$ and $L_{p,pk}$ in the unit of dB re 1μ Pa.

Scenarios	**SEL**	$\mathbf{L}_{p,pk}$
Noise prediction for the unmitigated field	180	199
Measurement sound levels	165 168	184 187
Measured noise reduction Δ_m	14 ∼17	14 ∼17
Perfectly noise cancelling	150	165
Non-fully noise cancelling (angular dependent, 0°)	153	179
Non-fully noise cancelling (angular dependent, 90°)	152	173
Non-fully noise cancelling (angular dependent, 180°)	153	178
Non-fully noise cancelling (angular dependent, 270°)	152	173
Maximum noise reduction level	30	34

circumference direction, a complete compressible flow model for predict air transportation from the air injection vessel to the hose is required. The model can be later coupled to the hydrodynamic model for describing the bubble formation and generation. It is worth investigating the angular dependence of the acoustic characteristic of the bubble curtain.

4. Conclusions

A three-dimensional boundary integral formulation is developed for the solution of the coupled vibro-acoustic problem in offshore pile driving. The developed model allows to examine the performance of the air-bubble curtains that can vary significantly in azimuth due to the inherent variations in the airflow circulation through the perforated pipes positioned on the seabed surface or other environmental conditions. The theoretical benchmark cases are compared against the numerical solution from FEM, the results prove the validity of the formulation given the excellent agreement between the two models. The ideal perfectly noise blockage is examined for an offshore pile driving foundation, which provides the maximum noise reduction potential. When a small gap is included through the BIE, it leads to a deviation of up to 1 dB for SEL and 6 dB for $L_{p,pk}$ as compared to the fully-blockage case. The measured levels indicate there is up to 3 dB variation in

azimuth during the installation with the use of DBBC system. To further investigate this phenomenon, the insertion loss of the bubble curtain system should be calculated based on the configuration of the system. The proposed formulation can be further implemented for arbitrary boundary conditions including three-dimensional wave field from pile driving or transmission losses varying in the circumference.

Acknowledgments
The authors also wish to express their thanks to Van Oord and specifically to Remco Huizer, Wouter Dirks, and Roeland Ris for supporting this research and for providing data from an offshore installation campaign in a recent year. For questions related to the data please contact the Noise Desk of Van Oord (NoiseDesk@vanoord.com).

References

[1] Bailey H, Senior B, Simmons D, Rusin J, Picken G and Thompson P M 2010 *Marine Pollution Bulletin* **60** 888–897 ISSN 0025-326X
[2] Hastie G, Merchant N D, Götz T, Russell D J F, Thompson P and Janik V M 2019 *Ecological Applications* **29** ISSN 1051-0761
[3] Stöber U and Thomsen F 2019 *J. Acoust. Soc. Am.* **145** 3252 ISSN 0001-4966
[4] Hastie G, Merchant N D, Götz T, Russell D J F, Thompson P and Janik V M 2019 *Ecological applications : a publication of the Ecological Society of America* **29** e01906 ISSN 1051-0761
[5] Verfuß T 2014 *Noise mitigation systems and low-noise installation technologies* (Wiesbaden : Springer Fachmedien Wiesbaden : Springer Spektrum) ISBN 978-3-658-02461-1 978-3-658-02462-8
[6] Tsouvalas A and Metrikine A V 2016 *Journal of Sound and Vibration* **371** 150–170 ISSN 0022-460X
[7] Reinhall P G and Dahl P H 2011 *J. Acoust. Soc. Am.* **130** 1209–16 ISSN 0001-4966
[8] Zampolli M, Nijhof M J, de Jong C A, Ainslie M A, Jansen E H and Quesson B A 2013 *J. Acoust. Soc. Am.* **133** 72–81 ISSN 0001-4966
[9] Lippert S, Nijhof M, Lippert T, Wilkes D, Gavrilov A, Heitmann K, Ruhnau M, von Estorff O, Schäfke A, Schäfer I, Ehrlich J, MacGillivray A, Park J, Seong W, Ainslie M A, de Jong C, Wood M, Wang L and Theobald P 2016 *IEEE Journal of Oceanic Engineering* **41** 1061–1071 ISSN 0364-9059 URL `http://ieeexplore.ieee.org/document/7458145/`
[10] Deng Q, Jiang W, Tan M and Xing J 2016 *Applied Acoustics* **104** 85–100 ISSN 0003-682X
[11] Lippert T, Ainslie M A and von Estorff O 2018 *J. Acoust. Soc. Am.* **143** 310 ISSN 0001-4966
[12] Peng Y, Tsouvalas A and Metrikine A V 2020 *The Journal of the Acoustical Society of America,*
[13] Bohne T, Grießmann T and Rolfes R 2019 *The Journal of the Acoustical Society of America* **146** 2212 ISSN 0001-4966
[14] Bohne T, Grießmann T and Rolfes R 2020 *International Journal of Multiphase Flow* **132** ISSN 0301-9322
[15] Peng Y, Tsouvalas A, Stampoultzoglou T and Metrikine A 2021 *Journal of Marine Science and Engineering* **9** ISSN 2077-1312
[16] Lippert S, Huisman M, Ruhnau M, Estorff O and van Zandwijk K 2017 Prognosis of underwater pile driving noise for submerged skirt piles of jacket structures *Proceedings of the UACE 2017 4th Underwater Acoustics Conference and Exhibition*
[17] Sertlek H O and Tsouvalas A 2022 Underwater sound propagation through an air-bubble medium in an acousto-elastic waveguide *Proceedings of the 28th International Congress on Sound and Vibration* ISBN 978-981-18-5070-7
[18] Göttsche K 2013 Numerical prediction of underwater noise reduction during offshore pile driving by a small bubble curtain *Proceedings of the International Congress and Exposition on Noise Control Engineering (INTER-NOISE), Innsbruck, Austria*
[19] Beelen S, van Rijsbergen M, Birvalski M, Bloemhof F and Krug D 2023 *Experiments in Fluids* **64** 31 ISSN 1432-1114 URL `https://doi.org/10.1007/s00348-022-03568-6`
[20] Aki K and Richards P G 2002 *Quantitative seismology* 2nd ed (Sausalito, Calif.: University Science Books) ISBN 0935702962 9780935702965
[21] Tsinopoulos S V, Agnantiaris J P and Polyzos D 1999 *The Journal of the Acoustical Society of America* **105** 1517–1526 URL `https://doi.org/10.1121/1.426691`
[22] OZKAN G O N C A and MENGI Y A L C I N 1997 *International Journal for Numerical Methods in Engineering* **40** 2385–2412